



INNOV 2025

The Fourteenth International Conference on Communications, Computation,
Networks and Technologies

ISBN: 978-1-68558-302-6

September 28th - October 2nd, 2025

Lisbon, Portugal

INNOV 2025 Editors

Petre Dini, IARIA, USA/EU

INNOV 2025

Forward

The Fourteenth International Conference on Communications, Computation, Networks and Technologies (INNOV 2025), held on September 28 – October 1, 2025 in Lisbon, Portugal, aimed at addressing recent research results and forecasting challenges on selected topics related to communications, computation, networks and technologies.

Considering the importance of innovative topics in today's technology-driven society, there is a paradigm shift in classical-by-now approaches, such as networking, communications, resource sharing, collaboration and telecommunications. Recent achievements demand rethinking available technologies and considering the emerging ones.

The conference had the following tracks:

- ☐ Communications
- ☐ Networking
- ☐ Computing
- ☐ Web Semantic and Data Processing
- ☐ Security, Trust, and Privacy

We take here the opportunity to warmly thank all the members of the INNOV 2025 technical program committee, as well as the numerous reviewers. The creation of such a high quality conference program would not have been possible without their involvement. We also kindly thank all the authors that dedicated much of their time and effort to contribute to INNOV 2025. We truly believe that, thanks to all these efforts, the final conference program consisted of top quality contributions.

Also, this event could not have been a reality without the support of many individuals, organizations and sponsors. We also gratefully thank the members of the INNOV 2025 organizing committee for their help in handling the logistics and for their work that made this professional meeting a success.

We hope that INNOV 2025 was a successful international forum for the exchange of ideas and results between academia and industry and to promote further progress in the areas of communication, computation, networks and technologies. We also hope that Lisbon provided a pleasant environment during the conference and everyone saved some time for exploring this beautiful city

INNOV 2025 Steering Committee

Sean Sturley, University of the West of Scotland, UK
Yeim-Kuan Chang, National Cheng Kung University, Taiwan

INNOV 2025 Publicity Chair

Lorena Parra Boronat, Universidad Politécnica de Madrid, Spain
Sandra Viciano Tudela, Universitat Politecnica de Valencia, Spain

Jose Miguel Jimenez, Universitat Politecnica de Valencia, Spain

Sourav Banerjee, Kalyani Government Engineering College, West Bengal, India

INNOV 2025

Committee

INNOV 2025 Steering Committee

Sean Sturley, University of the West of Scotland, UK
Yeim-Kuan Chang, National Cheng Kung University, Taiwan

INNOV 2025 Publicity Chair

Lorena Parra Boronat, Universidad Politécnica de Madrid, Spain
Sandra Viciano Tudela, Universitat Politecnica de Valencia, Spain
Jose Miguel Jimenez, Universitat Politecnica de Valencia, Spain
Sourav Banerjee, Kalyani Government Engineering College, West Bengal, India

INNOV 2025 Technical Program Committee

Lavanya Addepalli, Universitat Politecnica de Valencia, Spain
Akshit Aggarwal, Indian Institute of Information Technology Guwahati, India
Amjad Ali, University of Swat, Pakistan
Sourav Banerjee, Kalyani Government Engineering College, India
Eugen Borcoci, National University of Science and Technology POLITEHNICA Bucharest, Romania
Constantin F. Caruntu, Gheorghe Asachi Technical University of Iasi, Romania
YK Chang, National Cheng Kung University, Taiwan
DeJiu Chen, KTH Royal Institute of Technology, Sweden
Albert M. K. Cheng, University of Houston, USA
Karl Cox, University of Brighton, UK
Daniela D'Auria, Free University of Bozen-Bolzano, Italy
Panagiotis Fouliras, University of Macedonia, Thessaloniki, Greece
Marco Furini, University of Modena and Reggio Emilia, Italy
Laura García, Universitat Politècnica de València, Spain
Nikolaos Gorgolis, University of Patras, Greece
Victor Govindaswamy, Concordia University Chicago, USA
Jens Grambau, HdM Stuttgart, Germany
Qiang He, Swinburne University of Technology, Australia
Mehdi Hosseinzadeh, Washington University in St. Louis, USA
Shih-Chang Huang, National Formosa University, Taiwan
Wen-Jyi Hwang, National Taiwan Normal University, Taipei, Taiwan
Sergio Ilarri, University of Zaragoza, Spain
AKM Kamrul Islam, North Carolina A&T State University, USA
Brigitte Jaumard, Concordia University, Canada
Alexey Kashevnik, SPIIRAS, Russia
Sameh Kchaou, University of Sfax, Tunisia
Khaled Khankan, Taibah University, Saudi Arabia

Vasileios Komianos, Ionian University, Greece
Igor Kotenko, SPIIRAS, Russia
Boris Kovalerchuk, Central Washington University, USA
Maurizio Leotta, University of Genova, Italy
Yiu-Wing Leung, Hong Kong Baptist University, Hong Kong
Chanjuan Liu, Dalian University of Technology, China
Jaime Lloret, Universitat Politècnica de València, Spain
Bertram Lohmüller, SGIT | Steinbeis-Hochschule Berlin, Germany
René Meier, Hochschule Luzern, Switzerland
Souheir Merkouche, LIRE Laboratory | University of Constantine 2 - Abdelhamid Mehri, Algeria
Alfredo Milani, University of Perugia, Italy
Amalia Miliou, Aristotle University of Thessaloniki, Greece
Vincenzo Moscato, University of Naples "Federico II", Italy
Stylianos Mystakidis, School of Natural Sciences | University of Patras, Greece
Shin-ichi Ohnishi, Hokkai-Gakuen University, Japan
Ilias Panagiotopoulos, Harokopio University of Athens (HUA), Greece
Xingchao Peng, Boston University, USA
Ounsa Roudies, Ecole Mohammadia d'Ingénieurs - Mohammed-V University in Rabat, Morocco
Mohammad Shadravan, Yale University, USA
Sicong Shao, University of North Dakota, USA
Bowen Song, University of Southern California, USA
Sean Sturley, University of the West of Scotland, UK
Sheng Tan, Trinity University, USA
Ze Tang, Jiangnan University, China
J. A. Tenreiro Machado, Institute of Engineering of Porto | Polytechnic of Porto, Portugal
Christos Tjortjis, International Hellenic University, Greece
Raquel Trillo-Lado, University of Zaragoza, Spain
Christos Troussas, University of West Attica, Greece
Costas Vassilakis, University of the Peloponnese, Greece
Gerasimos Vonitsanos, University of Patras, Greece
Michael N. Vrahatis, University of Patras, Greece
Yuehua Wang, Texas A&M University-Commerce, USA
Alex Wijesinha, Towson University, USA
John R. Woodward, Queen Mary University of London, UK
Cong-Cong Xing, Nicholls State University, USA
Jason Zurawski, Lawrence Berkeley National Laboratory / Energy Sciences Network, USA

Copyright Information

For your reference, this is the text governing the copyright release for material published by IARIA.

The copyright release is a transfer of publication rights, which allows IARIA and its partners to drive the dissemination of the published material. This allows IARIA to give articles increased visibility via distribution, inclusion in libraries, and arrangements for submission to indexes.

I, the undersigned, declare that the article is original, and that I represent the authors of this article in the copyright release matters. If this work has been done as work-for-hire, I have obtained all necessary clearances to execute a copyright release. I hereby irrevocably transfer exclusive copyright for this material to IARIA. I give IARIA permission to reproduce the work in any media format such as, but not limited to, print, digital, or electronic. I give IARIA permission to distribute the materials without restriction to any institutions or individuals. I give IARIA permission to submit the work for inclusion in article repositories as IARIA sees fit.

I, the undersigned, declare that to the best of my knowledge, the article does not contain libelous or otherwise unlawful contents or invading the right of privacy or infringing on a proprietary right.

Following the copyright release, any circulated version of the article must bear the copyright notice and any header and footer information that IARIA applies to the published article.

IARIA grants royalty-free permission to the authors to disseminate the work, under the above provisions, for any academic, commercial, or industrial use. IARIA grants royalty-free permission to any individuals or institutions to make the article available electronically, online, or in print.

IARIA acknowledges that rights to any algorithm, process, procedure, apparatus, or articles of manufacture remain with the authors and their employers.

I, the undersigned, understand that IARIA will not be liable, in contract, tort (including, without limitation, negligence), pre-contract or other representations (other than fraudulent misrepresentations) or otherwise in connection with the publication of my work.


Exception to the above is made for work-for-hire performed while employed by the government. In that case, copyright to the material remains with the said government. The rightful owners (authors and government entity) grant unlimited and unrestricted permission to IARIA, IARIA's contractors, and IARIA's partners to further distribute the work.

Table of Contents

A Note on Structure Compatibility for Large Scale Structure Learning <i>Sung-Ho Kim and Namgil Lee</i>	1
---	---

Design, Operation, and Field Testing of MoBI: A Smart Buoy for Coastal Monitoring <i>Alessio Chirigu, Alberto Mancosu, Sara Pinna, Mariella Sole, Matteo Anedda, and Daniele Giusto</i>	5
--	---

A Note on Structure Compatibility for Large Scale Structure Learning

Sung-Ho Kim 

Department of Mathematical Sciences, Korea Advanced Institute of Science and Technology, Daejeon, S. Korea

e-mail: sungkim@kaist.ac.kr

Namgil Lee

Department of Information and Statistics, Kangwon National University, Chuncheon, S. Korea

e-mail: namgil.lee@kangwon.ac.kr

Abstract—Suppose that we are given two statistical model structures given in graphs. We are interested in testing whether they are from one source model or data. If the models share a source, we say that the models are compatible. In the paper, we present methods of testing compatibility of two model structures provided that the two structures share at least two nodes. The model structure represents causal or associative relationships between random variables (or nodes in graphs). Two testing methods will be proposed. One is by comparing structures of the intersection part of the two models, and the other is by using what we call union graphs. A union graph is obtained by merging the given structures with some additions and deletions of edges under a specified condition. We then check if the given structures are possible from the union graph. The methods are illustrated through examples. We aim to develop a method of structure learning by using as many pieces of structure information as possible. In this line of work, the pieces of information given in graphs need be checked for compatibility among themselves. This is the reason why this small piece of work is so crucial to the success of our future work.

Keywords—combined model structure; Markovian subgraph; structural discrepancy; union graph; combined model structure; Markovian subgraph; structural discrepancy; union graph.

I. INTRODUCTION

Independence graphs have been extensively used in multivariate data analysis to understand the Markov properties underlying joint distributions. In an independence graph, random variables are represented as nodes, where edges are absent between two nodes if the corresponding random variables are conditionally independent. This study focuses on undirected independence graphs, characterized by undirected edges and no predefined node ordering. For comprehensive overviews of independence graphs, see [1].

In scenarios involving two distinct data sources, where only part of a whole multivariate system can be observed from each source, it is necessary to combine models inferred separately from each source to construct a unified model for the entire system. We investigate the problem of combining two probabilistic graphical models, represented by their respective graph structures, into a single, larger graphical model. While substantial research has focused on combining Bayesian networks [2]–[4], comparatively less attention has been given to the combination of undirected graphical models. Notable exceptions include works addressing the combination of conditional log-linear model structures [5], studies on Markovian subgraphs under undirected decomposable graphical models [6], and strategies for combining decomposable

and non-decomposable undirected graphical model structures [7]. Further, Massa and Lauritzen [8] explored the properties of combined distribution families, applying their findings to Gaussian graphical models.

The computational complexity associated with searching for graphical model structures increases significantly with the number of variables. Thus, it is beneficial to check the feasibility of a joint model prior to undertaking computationally intensive procedures for combining marginal model structures. Dawid and Studeny [9] introduced the concept of compatibility for merging objects while preserving as much conditional independence as possible. Kim [7] defined graphical compatibility, for sets of graphical model structures using Markovian subgraphs.

This work proposes a novel methodology for testing the structure compatibility of two undirected graphical model structures, where the compatibility is defined in Definition 2.

The paper is organized in 4 sections. In Section 2, we introduce some notation and terminologies along with a few lemmas as preliminary to the main results. The relationship between probability models and graphs is briefly described. Section 3 is of main results proposed for testing structural incompatibility. In Section 4, we conclude the paper with remarks for summary and plans for future works.

II. PRELIMINARIES

The set of nodes in a graph G is denoted by $V(G)$, while the set of edges is denoted by $E(G)$. For a graph $G = (V, E)$ and two nodes $i, j \in V$, a path between i and j is a sequence of edges in E that connects i and j . For example, a path can be represented as $\{(i, v_1), (v_1, v_2), \dots, (v_{m-1}, j)\} \subset E$. For subsets of nodes $A_1, A_2 \subset V$, a path $\{(i, v_1), (v_1, v_2), \dots, (v_{m-1}, j)\}$ is an $A_2 \setminus A_1$ -path between i and j if $v_1, v_2, \dots, v_{m-1} \in A_2 \setminus A_1$.

For a graph $G = (V, E)$ and a subset of nodes $A \subset V$, the induced subgraph of G on A is defined as $G_A = (A, E \cap (A \times A))$. Another type of subgraph, called the Markovian subgraph, is defined as follows.

Definition 1 (Markovian subgraph [6]). *For a graph $G = (V, E)$ and a subset of nodes $A \subset V$, the Markovian subgraph of G upon A is defined as $G_{-A} = (A, E_{-A})$ such that*

$(i, j) \in E_{-A}$ if and only if $(i, j) \in E \cap (A \times A)$ or there exists a $V \setminus A$ -path between i and j .

If a graph G' is a Markovian subgraph of a graph G , we write as

$$G' \subset_M G \quad \text{or} \quad G \supset_M G'.$$

Before moving further, we need more notations. For a given graph $G' = (V', E')$ and a set of nodes $W \supset V'$, we define two sets of graphs as follows:

$$\begin{aligned} I^W(G') &= \{G \mid W \supset V(G) \supset V(G') \text{ such that, for } \{i, j\} \subseteq V(G'), (i, j) \notin E(G') \text{ implies that } (i, j) \notin E(G) \\ &\quad \text{and that there is no } V(G) \setminus V(G')\text{-path between } i \text{ and } j \text{ in } G\}. \\ D^W(G') &= \{G \mid W \supset V(G) \supset V(G') \text{ such that, for } \{i, j\} \subseteq V(G'), (i, j) \in E(G') \text{ implies that } (i, j) \in E(G) \\ &\quad \text{or that there is at least one } V(G) \setminus V(G')\text{-path between } i \text{ and } j \text{ in } G\}. \end{aligned}$$

The superset W is required only to set an upper bound on the node set so that the sets $I^W(G')$ and $D^W(G')$ are well-defined. The following lemma is immediate from Definition 1.

Lemma 1. *For graphs G and G' with $W \supset V(G) \supset V(G')$, $G \supset_M G'$ if and only if $G \in I^W(G') \cap D^W(G')$.*

We can now show that the Markovian subgraph relation is transitive as in

Lemma 2. *If $G \supset_M G' \supset_M G''$, then $G \supset_M G''$.*

Proof of Lemma 2. Assume that $G \supset_M G' \supset_M G''$. Let W be a set such that $W \supset V(G)$. Then we have from the assumption and Lemma 1 that $G \in I^W(G') \cap D^W(G')$ and that $G' \in I^W(G'') \cap D^W(G'')$. It suffices to show that $G \in I^W(G'') \cap D^W(G'')$.

Since $G' \in I^W(G'')$, for nodes i and j in $V(G'')$, $(i, j) \notin E(G'')$ implies that $(i, j) \notin E(G')$ and that there is no $V(G') \setminus V(G'')$ -path between i and j in G' . Since $G \in I^W(G')$, we can further derive that $(i, j) \notin E(G'')$ implies that $(i, j) \notin E(G)$ and that

there does not exist any $V(G') \setminus V(G'')$ -path between i and j in G' nor any $V(G) \setminus V(G'')$ -path between i and j in G . (1)

Statement (1) implies that there does not exist any $V(G) \setminus V(G'')$ -path between i and j in G : if the latter path exists, at least one of the two paths in statement (1) must exist by the definition of Markovian subgraph. Thus, we have $G \in I^W(G'')$.

From the condition of the lemma, we also have $G \in D^W(G')$ and $G' \in D^W(G'')$. It follows that $(i, j) \in E(G'')$ implies one of the following: either $(i, j) \in E(G)$, there exists a $V(G') \setminus V(G'')$ -path between i and j in G' , or there exists a $V(G) \setminus V(G'')$ -path between i and j in G . Since $V(G) \supset V(G') \supset V(G'')$, we can regard each of $V(G') \setminus V(G'')$ -path between i and j in G' and $V(G) \setminus V(G'')$ -path between i and j in G as a $V(G) \setminus V(G'')$ -path between i and j in G . , we have $G \in D^W(G'')$.

Therefore, it follows that $G \in I^W(G'') \cap D^W(G'')$, which completes the proof. \square

Since Markovian subgraphs are determined uniquely, we have

Lemma 3. *For a graph $G = (V, E)$ and two subsets of nodes A and B such that $A \subset B \subset V$, the following relationship holds:*

$$G_{-A} = (G_{-B})_{-A}.$$

We will briefly look into the relationship between probability models and graphs. For a given probability distribution P with its independence graph G , the relationship between a marginal probability distribution and a Markovian subgraph can be described as follows. A probability distribution P is said to be Markov with respect to G if P satisfies all the conditional independences (i.e., Markov properties) represented by G . The set of all probability distributions that are Markov with respect to G is denoted by $\mathcal{M}(G)$. If the joint distribution P satisfies the Markov properties associated with a graph G , then for any subset of nodes $A \subset V$, the marginal distribution P_A must satisfy the Markov properties expressed by the Markovian subgraph G_{-A} [7]. This relationship can be formally stated as follows.

Corollary 1 ([7]). *Let $G = (V, E)$ be an undirected graph, and suppose the distribution P of a random vector X_V satisfies $P \in \mathcal{M}(G)$. For a subset $A \subset V$, let $X_V = (X_A, X_{V \setminus A})$, and let P_A denote the marginal distribution of the random vector X_A . Then, the following holds:*

$$P_A \in \mathcal{M}(G_{-A}).$$

For two probability distributions $P_1 \in \mathcal{M}(G_1)$ and $P_2 \in \mathcal{M}(G_2)$, the P_1 and P_2 are said to be (strongly) compatible if there exists a joint probability distribution $P \in \mathcal{M}(G)$ for some undirected graph G , such that P_1 and P_2 are the marginal distributions of P [9]. Using Corollary 1, the concept of compatibility for probability distributions can be extended to the compatibility of graph structures as follows.

Definition 2 (Structure Compatibility). *Two undirected graphs G_1 and G_2 are said to be compatible if there exists a graph G such that G_1 and G_2 are Markovian subgraphs of G .*

Further terminologies related to combined models are introduced below.

Definition 3 (Combined Model Structure (CMS) [7]). *A graph $G = (V, E)$ is referred to as a combined model structure (CMS) of two graphs $G_1 = (V_1, E_1)$ and $G_2 = (V_2, E_2)$ if $V = V_1 \cup V_2$ and G_1 and G_2 are Markovian subgraphs of G . A CMS is called maximal if adding any additional edge results in a graph that is no longer a CMS. The set of all maximal CMSs of G_1 and G_2 is denoted by $G_1 \oplus G_2$.*

It is obvious that the concepts of structure compatibility and existence of a CMS are equivalent.

III. MAIN RESULTS

In this section, we devise rules for testing incompatibility between graphs by applying graph theory and Markov properties. To avoid trivial cases, we assume that two graphs share at least two nodes. Consider two graphs, $G_1 = (V_1, E_1)$ and $G_2 = (V_2, E_2)$, for which $C = V_1 \cap V_2$ and $|C| \geq 2$.

A. Checking Discrepancy in intersection part

The first of our methods of compatibility test is by comparing $(G_1)_C$ and $(G_2)_C$. It is intuitive that, if the two Markovian subgraphs G_1 and G_2 on C are not the same, G_1 and G_2 are not from the same model structure. This observation is stated formally as follows.

Theorem 1. For graphs G_1 and G_2 with $C = V_1 \cap V_2$, if $(G_1)_C \neq (G_2)_C$, then $G_1 \oplus G_2 = \emptyset$.

Proof of Theorem 1. Suppose there exists a graph $G = (V, E)$ such that G_1 and G_2 are Markovian subgraphs of G . Then, by Lemma 3, we have $(G_1)_C = G_C = (G_2)_C$. This contradicts the condition of the theorem, implying that G_1 and G_2 cannot have a Markovian supergraph such as G . From this follows the desired result that $G_1 \oplus G_2 = \emptyset$. \square

An example of the two graphs that satisfy the condition of this theorem is given in Figure 1. We can easily check that the Markovian subgraphs G_1 and G_2 of G in the figure satisfy the equality $(G_1)_C = (G_2)_C$ for $C = \{3, 4, 5, 6, 7\}$. However, the other two graphs G'_1 and G'_2 , which were obtained by removing the edges $(4, 5)$ from G_1 and $(6, 8)$ from G_2 , are not compatible according to Theorem 1.

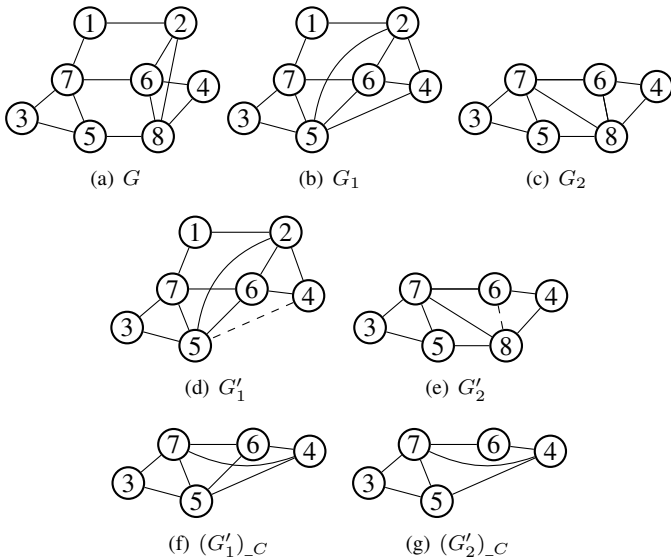


Figure 1. Two graphs, G'_1 and G'_2 , satisfying the condition of Theorem 1. For a graph G , its Markovian subgraphs G_1 and G_2 are obtained upon the node sets $A = \{1, 2, \dots, 7\}$ and $B = \{3, 4, \dots, 8\}$ respectively. Edge $(4, 5)$ is removed from G_1 into G'_1 and edge $(6, 8)$ is removed from G_2 into G'_2 . The removed edges are dashed in G'_1 and G'_2 . For the set $C = A \cap B$, $(G'_1)_C \neq (G'_2)_C$.

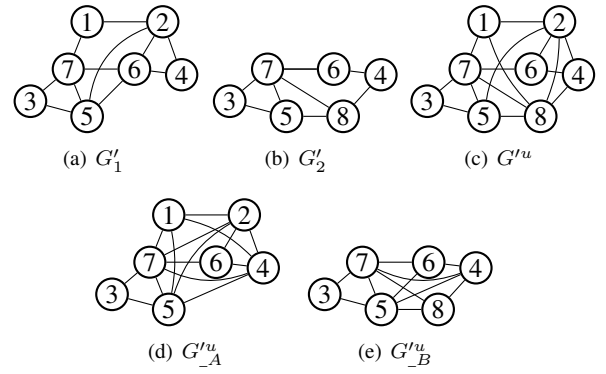


Figure 2. An example where a Markovian subgraph of union(G_1, G_2) does contain none of G_1 and G_2 as a subgraph. G'_1 and G'_2 are carried over from Figure 1 with dashed edges erased. G'^u_A and G'^u_B are Markovian subgraphs of G'^u upon A and B respectively. Note that $G'^u_A \not\subseteq G'^u_B$.

B. Using Union Graphs

A union graph, $G^u = \text{union}(G_1, G_2)$, of two graphs G_1 and G_2 is defined as $G^u = (V^u, E^u)$ where $V^u = V_1 \cup V_2$ and $(i, j) \in E^u$ if and only if either $(i, j) \in E_1 \cap E_2$ or $i \in V_1 \setminus V_2$ and $j \in V_2 \setminus V_1$. That is, a union graph is formed by adding edges between nodes in $V_1 \setminus V_2$ and those in $V_2 \setminus V_1$ [7].

The following lemma provides a theoretical basis for testing incompatibility using union graphs.

Lemma 4. For a graph $G = (V, E)$, let A and B be subsets of V such that $A \cup B = V$. Then

$$G \subseteq \text{union}(G_{-A}, G_{-B}).$$

Proof of Lemma 4. $G_A \subseteq G_{-A}$ and $G_B \subseteq G_{-B}$. Thus, it follows that $G \subseteq \text{union}(G_A, G_B) \subseteq \text{union}(G_{-A}, G_{-B})$. \square

Theorem 2. Let $G^u = \text{union}(G_1, G_2)$ and $V_i = V(G_i)$ for $i = 1, 2$. If there exists i such that $G_i \not\subseteq (G^u)_{-V_i}$, then $G_1 \oplus G_2 = \emptyset$.

Proof of Theorem 2. Suppose that $G_1 \oplus G_2 \neq \emptyset$ and let H be a graph in $G_1 \oplus G_2$. Then, by Lemma 4, $H \subseteq G^u = \text{union}(G_1, G_2)$. Since $G_i \subseteq H_{-V_i}$ for $i = 1, 2$, we have $G_i \subseteq (G^u)_{-V_i}$ for $i = 1, 2$, which contradicts the condition of the theorem.

Therefore, under the condition of the theorem, it must hold that $G_1 \oplus G_2 = \emptyset$. \square

An example of this theorem is given in Figure 2 where G'_1 and G'_2 are carried over from Figure 1 with dashed edges erased. After constructing the union graph G'^u of G'_1 and G'_2 , we checked if $G'_i \subseteq G'^u_{-V_i}$ holds and found that $G'_1 \not\subseteq G'^u_{-A}$ and $G'_2 \subseteq G'^u_{-B}$.

For any two graphs G_1 and G_2 with $V(G_i) = V_i$, $i = 1, 2$, and $C = V_1 \cap V_2$, the discrepancy, $(G_1)_C \neq (G_2)_C$, does not necessarily imply existence of $i \in \{1, 2\}$ such that $G_i \not\subseteq \text{union}(G_1, G_2)_{-V_i}$. For G_1 and G_2 in Figure 3 with $C = \{1, 2, 3\}$, we have $(G_1)_C \neq (G_2)_C$ but

$$G_i \subseteq \text{union}(G_1, G_2)_{-V_i} \text{ for } i = 1, 2. \quad (2)$$

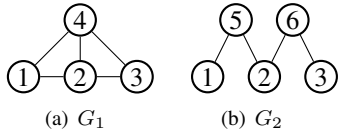


Figure 3. An incompatible pair of graphs. The incompatibility of this pair is confirmed by Theorem 1 but not by Theorem 2.

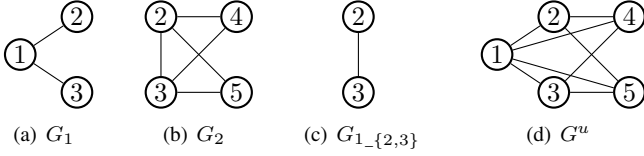


Figure 4. Two graphs G_1 and G_2 , the Markovian subgraph $G_{1_{\{2,3\}}}$ on the common nodes 2 and 3, and the union graph G^u .

However, $(G_1)_C = (G_2)_C$ has much to do with (2) as shown below.

Theorem 3. For two graphs G_i , $i = 1, 2$, let $V_i = V(G_i)$ and $C = V_1 \cap V_2$. If $(G_1)_C = (G_2)_C$, then (2) holds true.

Proof of Theorem 3. Let E^* be the set of the edges whose nodes are in C only and each of which appears in only one of G_1 or G_2 . We will denote by G^+ the graph whose node and edge sets are given respectively by $V^+ = V_1 \cup V_2$ and $E^+ = E(G_1) \cup E(G_2) \setminus E^*$. Then, under the condition of the theorem, we have

$$G_{V_i}^+ = G_i, \text{ for } i = 1, 2. \quad (3)$$

Note that $G_{V_i}^+$ is obtained by adding to the induced subgraph G_C^+ of G^+ all the edges in $E((G_i)_C) \setminus E(G_C^+)$. This is why we have the above equation.

By definition, $G^+ \subseteq \text{union}(G_1, G_2)$, since $\text{union}(G_1, G_2)$ is obtained by adding to G^+ all the edges between the nodes in $V_1 \setminus C$ and those in $V_2 \setminus C$. From this follows the desired result (2). \square

We can see an example of this theorem in Figure 4. In the figure, $V_1 = \{1, 2, 3\}$, $V_2 = \{2, 3, 4, 5\}$, and $C = \{2, 3\}$. We have $(G_1)_C = (G_2)_C$ and $G_i \subseteq G_{V_i}^+$, $i = 1, 2$. Note however in the figure that G_1 and G_2 are not compatible. This simple example indicates that the conditions of Theorems 1 and 2 are sufficient for incompatibility of a pair of graphs but not necessary.

IV. CONCLUSION AND FUTURE WORK

In this work, we presented two methods for incompatibility test. One of them is by checking structural discrepancy in the intersection part of two model structures and the other is by using union graphs. If any of the given graphs is not contained in the corresponding Markovian subgraph of the union graph, we may conclude that the graphs are not compatible.

The methods are devised based on graph and statistical theories. If the graphs are incompatible, it means that they are not from a unified graph. If we regard the graphs as

model structures, the incompatibility implies that the models are not from a source of data. Experiments show that these testing methods are very useful in large scale structure learning since we can save our time in structure learning by avoiding incompatible model structures at the early stage of structure learning.

This work is yet an early stage of large scale statistical (structure) learning from big data. We will search for more methods for incompatibility test, then we will develop methods for using pieces of structure information obtained from different sets of data towards the large scale learning.

Kim and Kim[4] used pieces of structural information for structure learning and improved preceding learning methods. We aim to develop a method of structure learning by using as many pieces of structure information as possible. In this line of work, the pieces of information given in graphs need be checked for compatibility among themselves. In this way we could keep the quality of the structure information at a high level.

ACKNOWLEDGEMENTS

This work was supported by National Research Foundation of Korea (NRF) grants funded by the Korea government (MSIT) (No. RS-2024-00358572, No. RS-2024-00336424).

REFERENCES

- [1] S. L. Lauritzen, *Graphical Models*. Oxford, UK: Clarendon Press, 1996.
- [2] D. Danks, C. Glymour, and R. Tillman, "Integrating locally learned causal structures with overlapping variables," in *Advances in Neural Information Processing Systems*, D. Koller, D. Schuurmans, Y. Bengio, and L. Bottou, Eds., vol. 21, Curran Associates, Inc., 2008.
- [3] S. Triantafillou and I. Tsamardinos, "Constraint-based causal discovery from multiple interventions over overlapping variable sets," *Journal of Machine Learning Research*, vol. 16, no. 66, pp. 2147–2205, 2015.
- [4] G. Kim and S. Kim, "Marginal information for structure learning," *Statistics and Computing*, vol. 430, no. 30, pp. 331–349, 2020. DOI: 10.1007/s11222-019-09877-x.
- [5] S. E. Fienberg and S.-H. Kim, "Combining conditional log-linear structures," *Journal of the American Statistical Association*, vol. 94, no. 445, pp. 229–239, 1999. DOI: 10.1080/01621459.1999.10473838.
- [6] S.-H. Kim, "Properties of Markovian subgraphs of a decomposable graph," in *MICAI 2006: Advances in Artificial Intelligence*, A. Gelbukh and C. A. Reyes-Garcia, Eds., Berlin, Heidelberg: Springer Berlin Heidelberg, 2006, pp. 15–26. DOI: 10.1007/11925231_2.
- [7] S.-H. Kim, "Learning model structures based on marginal model structures of undirected graphs," KAIST, BK21 Research Report 09-04, Mar. 2009.
- [8] M. S. Massa and S. L. Lauritzen, "Combining statistical models," in *Algebraic methods in statistics and probability II*, ser. Contemporary Mathematics, M. A. G. Viana and H. P. Wynn, Eds., Providence, RI: American Mathematical Society, 2010, pp. 239–259.
- [9] A. P. Dawid and M. Studený, "Conditional products: An alternative approach to conditional independence," in *Proceedings of the Seventh International Workshop on Artificial Intelligence and Statistics*, D. Heckerman and J. Whittaker, Eds., ser. Proceedings of Machine Learning Research, vol. R2, PMLR, 1999, pp. 27–35.

Design, Operation, and Field Testing of MoBI: A Smart Buoy for Coastal Monitoring

Alessio Chirigu¹, Alberto Mancosu¹, Sara Pinna², Mariella Sole¹, Matteo Anedda², and Daniele D Giusto²

¹hedy srl - Cagliari, Italy

²University of Cagliari, Department of Electrical and Electronic Engineering - UdR CNIT Cagliari, Cagliari, Italy

Abstract—This paper presents a smart buoy system designed for monitoring environmental conditions in coastal and marine areas. The proposed solution addresses the need for reliable, in situ data collection through the use of embedded hardware, multi-parameter sensors, and redundant communication technologies. This contribution aligns with the conference topics on intelligent sensing and autonomous systems for environmental applications. The work introduces a novel system architecture and reports original field test results obtained during real missions. The paper concludes that the system is robust and scalable, and that it offers a practical approach for improving data quality and transmission reliability in marine monitoring scenarios.

Keywords—smart buoy; environmental monitoring; LoRaWAN; LTE; marine data.

I. INTRODUCTION

Marine environmental monitoring represents a central challenge for the sustainable management of natural resources and the prevention of risks related to climate change and human activity. The EcoMonitoring project addresses this challenge by proposing an integrated solution based on autonomous buoys and surface drones, aimed at collecting environmental data in an efficient, scalable, and low-impact way [1].

The Monitoring Buoy Interface (MoBI) is one of the key components of this system. Constructed from Three-Dimensional (3D) printed High-Density Poly-Ethylene (HDPE), MoBI is designed to operate in a semi-autonomous mode, towed by an Unmanned Surface Vehicle (USV) to predefined positions where it performs targeted environmental measurements. Equipped with sensors for wave dynamics and water quality parameters, the buoy is capable of acquiring, processing, and transmitting data even under limited connectivity conditions, following an approach consistent with other recently proposed intelligent environmental monitoring systems [2].

This paper provides a detailed description of the MoBI system, including its architecture, operational logic, communication methods, and the results obtained from field testing. The following section outlines the system hardware and communication strategy, followed by a description of the data acquisition subsystems and, finally, an analysis of the field test campaigns and experimental results.

The remainder of the paper is organized as follows: Section II presents the hardware and software architecture of the MoBI system, including communication strategies and control logic. Section III details the environmental data acquisition process using the multi-parameter probe. Section IV focuses on the wave monitoring subsystem and its signal processing approach. Section V reports on the field test campaigns and discusses

the observed performance. Finally, Section VI provides the conclusion and outlines future developments.

II. SYSTEM DESIGN AND ARCHITECTURE

The MoBI system has been developed with the goal of providing a robust, modular, and economically sustainable solution for autonomous environmental monitoring in coastal and marine contexts. Its architecture combines low-power embedded processing, real-time interfacing with multiple sensors, and a dual communication strategy to ensure data integrity even under limited or absent connectivity conditions.

At the core of the system are two processing units: a Raspberry Pi 3B+ microcomputer and an Arduino Mega 2560 R3 microcontroller. These components are co-located inside the watertight structure of the buoy and are powered by a regulated circuit that provides 5V to the system. A step-up converter is used to generate the 12V required by the multiparameter probe.

The Raspberry Pi handles high-level operations, including communication with the multiparameter probe, data formatting, and log file generation. The Arduino, on the other hand, manages low-level data acquisition from inertial and positioning sensors, including Global Positioning System (GPS), accelerometer, gyroscope, and magnetometer, as well as the operation of the Long Range (LoRa) module for fallback data transmission.

Communication and synchronization between the Raspberry Pi and Arduino Mega take place via a Universal Serial Bus (USB) serial connection, which enables bidirectional exchange of data and commands between the two boards. This setup also allows the Arduino Mega to be powered directly through the Raspberry Pi using the same USB cable employed for data transmission, thereby simplifying the overall system wiring.

The communication protocol used is Universal Asynchronous Receiver-Transmitter (UART), a full-duplex asynchronous protocol that enables simultaneous transmission and reception of data through two separate channels. In a traditional UART connection, the Transmit (TX) pin of one device is connected to the Receive (RX) pin of the other, and vice versa. In the case of a USB connection, this link occurs indirectly, as each device includes a USB-to-Serial converter chip that translates UART signals into data compatible with the USB protocol, and vice versa. This communication is managed by dedicated software libraries.

Being an asynchronous protocol, UART does not require a shared clock between devices. To ensure correct communica-

tion, both devices must be configured with the same baud rate, i.e., the number of bits transmitted per second. This parameter is defined during software initialization.

On the Arduino Mega side, communication is handled using the Serial library, which allows the use of the four available hardware serial ports. The USB port is associated with Serial0, which uses pins 0 (RX) and 1 (TX), leaving the other ports free for connection with additional modules (for example, one is dedicated to the GPS module).

On the Raspberry Pi side, the pySerial Python library is used to access the serial port via USB and to manage the asynchronous exchange of commands in American Standard Code for Information Interchange (ASCII) format. This lightweight approach enables efficient synchronization between the two devices, avoiding system overload and ensuring smooth coordination of operations such as data acquisition, storage, and transmission.

To ensure continuous data transmission, MoBI implements a dual communication strategy. When Fourth Generation / Long-Term Evolution (4G/LTE) connectivity is available, the Raspberry Pi sends structured environmental data to a remote server. In the case of weak or absent signal, data are transmitted via LoRa [3]–[5]. The communication strategy is based on the combined use of 4G/LTE and LoRa, selected for their complementary characteristics in terms of bandwidth, coverage, and energy efficiency.

4G/LTE was chosen as the main transmission channel because it offers high data throughput, low latency, and broad coverage in most coastal and inland regions, enabling reliable and timely communication with remote servers.

LoRa was integrated as a fallback option to ensure data transmission in areas with limited or no cellular coverage. Its low energy consumption and long-range capabilities make it particularly suitable for transmitting environmental data in remote or hard-to-reach locations.

This dual approach increases the robustness and adaptability of the system, ensuring operational continuity and efficient data transfer across different deployment scenarios. In both cases, data are saved locally to a Secure Digital (SD) card to allow later transmission in the event of fallback failure. The system automatically verifies at the end of each mission whether the platform successfully received the data and, if needed, initiates retransmission via 4G.

The power system consists of a charge regulator and voltage converters (12V, 5V, 3.3V), supporting all connected electronic modules.

From a mechanical perspective, the MoBI buoy (shown in Figure 1) is made of 3D-printed HDPE. Its modular structure allows for easy maintenance and component replacement or upgrades, while the internal layout ensures watertight protection of the electronics, optimal antenna exposure (LTE, GPS, and LoRa), and proper probe immersion.

The system firmware was developed in Python (for Raspberry Pi) and C++ (for Arduino), following a finite-state machine logic to manage the mission flow. Each mission includes the following phases: sensor and communication initialization,



Figure 1. MoBI buoy.

movement to the acquisition points, data collection, and transmission. Figure 2 shows the complete operational software scheme of MoBI.

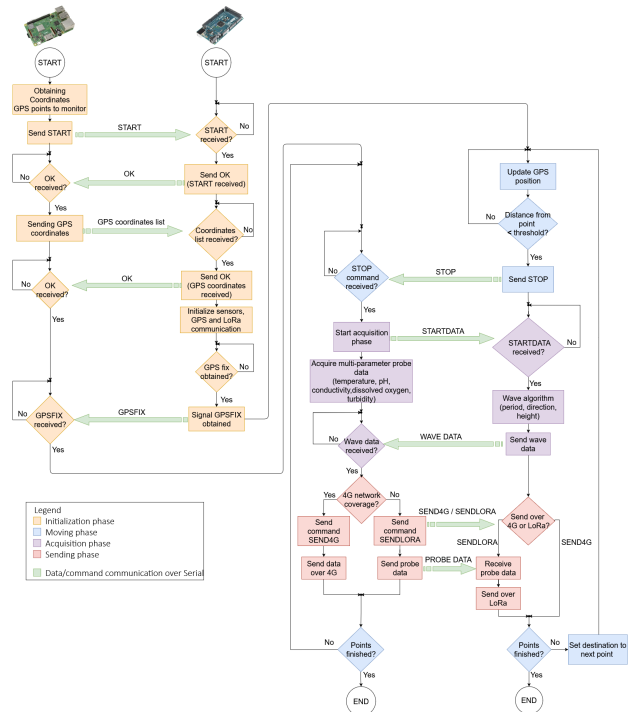


Figure 2. Software design.

At system startup, serial communication is established between the Arduino Mega and the Raspberry Pi, which is necessary for the continuous exchange of commands and data.

The mission begins with a request to the remote platform to obtain the GPS coordinates of the measurement points. Once the start command (START) is received, the Raspberry Pi retrieves the coordinates and transmits them to the Arduino.

After confirming successful reception, the Arduino proceeds with the initialization of the inertial sensors, the GPS module, and the LoRa communication. At the end of this phase, once a valid GPS fix is obtained, the Arduino sends a completion signal (GPSFIX), indicating that it is ready to start the mission.

Once initialization is complete, the system enters the navigation phase: the smart buoy (which may be towed manually or via USV) moves toward the first measurement point. During this phase, the Arduino Mega continuously updates the GPS position and compares the distance to the target point. When the distance falls below the configured threshold, the system sends the STOP command to the Arduino to indicate that the target has been reached and to proceed to the next phase.

The acquisition phase then follows: the Raspberry Pi sends the start command (STARTDATA) to the Arduino to initialize the wave motion analysis algorithm. From this moment on, inertial parameters related to wave period, direction, and height are recorded for a predefined duration.

In parallel, the Raspberry Pi collects data from the environmental probe, which measures parameters such as temperature, pH, conductivity, dissolved oxygen, and turbidity.

At the end of the acquisition, the Arduino transmits the wave data to the Raspberry Pi, thereby completing the data collection phase.

The data gathered by both units are then handled during the transmission phase, which depends on the available connectivity: if a 4G network is present, the data is sent immediately via the mobile network (SEND4G); otherwise, it is transmitted via LoRa to the receiving node (SENDLORA).

After transmission, the system checks whether there are additional points to visit. If so, it sets the next target and repeats the entire cycle. If all points have been visited, the mission is concluded.

The transmission frequency is variable and depends on the number of configured measurement points. Specifically, one data transmission is performed for each point.

III. ENVIRONMENTAL DATA ACQUISITION

The MoBI system is designed to collect two main categories of data: physical-chemical parameters of the water and wave-related measurements. The entire acquisition process is organized in automated cycles, ensuring both data integrity and compatibility with the transmission and storage systems.

For the acquisition of environmental data, the buoy is equipped with a multiparameter probe, model WMP6, connected to the Raspberry Pi via an Recommended Standard 485 (RS485) USB serial interface. This probe is capable of measuring several key water quality parameters in real time, including temperature, pH, electrical conductivity, dissolved oxygen, and turbidity. The probe remains immersed throughout the mission, ensuring continuous exposure to the environmental conditions being measured.

The acquisition cycle involves the Raspberry Pi sending read command sequences to the probe. The received data are processed using a software module based on regular expressions, allowing extraction and validation of each individual value.

For each parameter, the system performs three consecutive readings spaced a few seconds apart; the resulting values are then averaged and stored in a structured JavaScript Object Notation (JSON) file, ready for transmission or local archiving. Similar open-source and modular architectures have already been adopted in long-term water monitoring projects [6].

Special attention has been given to the management of turbidity, a parameter that often proves critical in saltwater testing. In some cases, the probe has returned anomalous or negative values during the initial moments of immersion. For this reason, a stabilization period was introduced before the actual sampling begins, to ensure representative measurements.

Collected data are saved to an SD card and simultaneously queued for transmission to the remote server via 4G/LTE network. In the absence of a network, the LoRa channel is used as a fallback. In both cases, the use of local SD storage ensures data availability for retransmission in case the initial transfer fails. At the end of each measurement cycle, the system verifies whether all data points have been successfully received by the platform and, if needed, selectively retransmits any missing data. Each measurement is timestamped and associated with GPS coordinates and a mission identifier code.

The acquisition cycle can be executed for each measurement point pre-configured on the web platform or triggered manually in the field. The flexibility of the system allows it to adapt to various operational scenarios, from short missions with a few points to extended campaigns involving dozens of successive readings.

IV. WAVE MOTION DETECTION

In addition to the physical-chemical parameters of the water, MoBI is capable of detecting the dynamic characteristics of wave motion, which are essential for coastal stability analysis and navigation safety. This functional module relies on a combination of inertial sensors (accelerometer and gyroscope) mounted on an X-NUCLEO-IKS01A3 board, integrated with a magnetometer for directional orientation.

The wave detection algorithm is based on a four-phase model, designed to identify full wave cycles through the analysis of vertical acceleration. Specifically, the system monitors variations along the Z-axis to detect acceleration and deceleration phases during both the rising and falling parts of the wave.

Once a complete wave cycle is detected, the system calculates the time interval between two consecutive peaks to estimate the wave period. The amplitude is estimated via double numerical integration of the accelerometer signal. Although this method introduces a degree of error due to sensor noise and drift, the results are sufficiently accurate for operational field use. A similar approach has also been adopted in professional systems for wave monitoring in coastal environments [7].

Wave motion data are acquired over a predefined period, configurable at the start of each measurement campaign. The results are averaged to ensure a representative statistical profile while avoiding overloading the transmission system. Like other

environmental data, wave parameters are georeferenced and stored in JSON format, ready for subsequent processing.

Field test campaigns have shown that the system can reliably detect waves greater than 5–10 cm in height, even in the presence of minor disturbances or buoy oscillations. This behavior is consistent with findings from low-cost prototype devices tested in lagoon environments [8]. However, a slight imprecision was observed in estimating wave periods under particularly calm conditions, due to difficulties in distinguishing buoy micro-movements from actual incident waves. Optimizations of the algorithm are planned to reduce this ambiguity.

V. TEST CAMPAIGN AND EXPERIMENTAL RESULTS

To validate the functionalities of the MoBI system under real operating conditions, a field test campaign was carried out between January and March 2025 in the area surrounding Cagliari, with particular focus on the Sant’Elmo pier and the Palma channel. The goal was to evaluate the system’s stability, the quality of the collected data, and the reliability of the communication subsystems in coastal scenarios characterized by variable environmental dynamics.

We first present the objectives and methodology of the testing activities, followed by a summary of the main experimental results.

A. Objectives and Methodology

The tests focused on verifying several key aspects of the system:

- GPS positioning accuracy during missions;
- Correct acquisition and structuring of environmental data;
- Robustness of 4G/LTE communications and fallback capability via LoRa;
- Behavior of the multiparameter probe in saline environments;
- Integration of the platform with backend systems (dashboard and storage).

During the operations, the buoy was transported to the target locations and kept stationary to enable data acquisition. Each cycle included coordinate logging, stabilization of the probe, and repeated sampling. Acquired data were transmitted in real-time when a 4G connection was available, or alternatively through LoRa when the primary connection was unavailable.

B. Main Results

Positioning. The GPS module showed an average error of approximately 10 meters relative to the configured targets. Although this deviation is within the platform’s operational limits, the use of a Global Navigation Satellite System (GNSS) module in later tests helped reduce both the fix acquisition time and average positioning error.

Environmental Data Quality. The multiparameter probe returned consistent values across all parameters, except for turbidity, which occasionally produced null or negative readings. In response, invalid values (such as negative turbidity) were discarded to preserve data integrity.

Communication Reliability. The system successfully transmitted data over LTE in areas with good coverage. During

periods without network access, the fallback and retransmission logic worked as expected: data were stored locally and later sent via LoRa. At the end of the mission, the system correctly checked the presence of any missing data by querying the platform. If any records were absent, they were retrieved from the SD card and retransmitted via 4G until confirmation of successful reception.

Integration and Visualization. The collected data were later imported into a cloud-based visualization and aggregation platform, where they were converted into interactive graphs and geospatial representations. Dashboards allowed real-time visualization of parameters, such as temperature, pH, and dissolved oxygen, giving operators direct control over water quality. The combined use of LoRa and a cloud dashboard has also been validated in professional systems, such as the CB-150 buoy deployed in Green Bay [9].

Operational Observations. From a logistical standpoint, the field deployment of the buoy confirmed the practicality of its modular design, which facilitated post-mission inspection and battery recharging. No hardware failures or water ingress were observed, confirming the watertight integrity of the 3D-printed HDPE structure.

VI. CONCLUSION AND FUTURE WORK

The MoBI system has proven to be a reliable, flexible, and suitable platform for environmental monitoring in marine and coastal settings. Its dual-processor architecture, integrated sensor suite, and redundant communication strategy enabled the system to effectively overcome the operational challenges encountered in the field.

The test campaigns confirmed the system’s robustness in terms of data acquisition, transmission, and backend integration. In most cases, the environmental measurements were consistent and stable. The wave analysis module delivered satisfactory performance for wave heights above 5 cm, while the software infrastructure ensured data logging and recovery even during periods of temporary network unavailability.

The experience gained during the field trials also highlighted several areas for improvement, which will guide future developments:

- improved power management to optimize consumption [10];
- further testing in more demanding wave conditions;
- extension of support for additional sensor protocols and automated long-term mission handling;
- native integration with cloud platforms for historical analysis and real-time alert generation.

Overall, MoBI represents a concrete step toward the automation of environmental monitoring, combining technological reliability with ease of use in a compact system ready for operational deployment in real coastal scenarios.

ACKNOWLEDGMENT

This research activity was partially funded by the European Union - NextGenerationEU and by the Ministry of University and Research (MUR), National Recovery and Resilience Plan (NRRP), Mission 4, Component 2, Investment 1.5, project

“RAISE - Robotics and AI for Socio-economic Empowerment” (ECS00000035).

REFERENCES

- [1] H. Bates, M. Pierce, and A. Benter, “Real-time environmental monitoring for aquaculture using a lorawan-based iot sensor network”, *Sensors*, vol. 21, no. 23, 2021, ISSN: 1424-8220. DOI: 10.3390/s21237963.
- [2] F. Li, Y. Shi, H. Li, Y. Yang, and P. Li, “Design and implementation of multi-parameter intelligent monitoring system for marine ranching”, in *Proceedings of the 2017 International Conference on Material Science and Engineering (ICMSE 2017)*, 2017, pp. 379–383. DOI: 10.2991/icmse-17.2017.72.
- [3] A. Majumder, M. Losito, S. Paramasivam, A. Kumar, and G. Gatto, “Buoys for marine weather data monitoring and lorawan communication”, *Ocean Engineering*, vol. 313, 119521, 2024. DOI: 10.1016/j.oceaneng.2024.119521.
- [4] A. Benjamin *et al.*, “Allora: Empowering environmental intelligence through an advanced lora-based iot solution”, *Computer Communications*, vol. 218, pp. 44–58, Mar. 2024. DOI: 10.1016/j.comcom.2024.02.014.
- [5] P. Sara *et al.*, “Evaluating lorawan connectivity in a marine scenario”, *Journal of Marine Science and Engineering*, vol. 9, p. 1218, Nov. 2021. DOI: 10.3390/jmse9111218.
- [6] Q. Quevy *et al.*, “Open sensing system for long term, low cost water quality monitoring”, *IEEE Open Journal of the Industrial Electronics Society*, vol. PP, pp. 1–16, Jan. 2023. DOI: 10.1109/OJIES.2022.3233919.
- [7] J. F. Martínez-Osuna *et al.*, “Coastal buoy data acquisition and telemetry system for monitoring oceanographic and meteorological variables in the gulf of mexico”, *Measurement*, vol. 183, p. 109841, 2021, ISSN: 0263-2241. DOI: <https://doi.org/10.1016/j.measurement.2021.109841>.
- [8] F. Campagnaro *et al.*, “Monitoring the venice lagoon: An iot cloud-based sensor network approach”, *IEEE Journal of Oceanic Engineering*, vol. PP, pp. 1–13, Jan. 2024. DOI: 10.1109/JOE.2024.3459483.
- [9] NexSens Technology, *Using data buoys to monitor southern green bay*, [retrieved: June, 2025], n.d.
- [10] C. Delgado, J. M. Sanz, C. Blondia, and J. Famaey, “Batteryless LoRaWAN communications using energy harvesting: Modeling and characterization”, *IEEE Internet of Things Journal*, vol. 8, no. 4, pp. 2694–2711, Feb. 2021. DOI: 10.1109/JIOT.2020.3019140.